Ann. Geophys., 31, 1611–1617, 2013
www.ann-geophys.net/31/1611/2013/
doi:10.5194/angeo-31-1611-2013

Annales Geophysicae
Open Access

Determination of wave vectors using the phase differencing method

S. N. Walker[1] **and I. Moiseenko**[2]

[1]Department of Automatic Control and Systems Engineering, University of Sheffield, Sheffield, UK
[2]Space Research Institute of the Russian Academy of Sciences, Moscow, Russia

Correspondence to: S. Walker (simon.walker@sheffield.ac.uk)

Received: 25 February 2013 – Revised: 29 May 2013 – Accepted: 17 August 2013 – Published: 27 September 2013

Abstract. Due to the collisionless nature of space plasmas, plasma waves play an important role in the redistribution of energy between the various particle populations in many regions of geospace. In order to fully comprehend such mechanisms it is necessary to characterise the nature of the waves present. This involves the determination of properties such as wave vector $\boldsymbol{k}$. There are a number of methods used to calculate $\boldsymbol{k}$ based on the multipoint measurements that are now available. These methods rely on the fact that the same wave packet is simultaneously observed at two or more locations whose separation is small in comparison to the correlation length of the wave packet. This limitation restricts the analysis to low frequency (MHD) waves. In this paper we propose an extension to the phase differencing method to enable the correlation of measurements that were not made simultaneously but differ temporally by a number of wave periods. The method is illustrated using measurements of magnetosonic waves from the Cluster STAFF search coil magnetometer. It is shown that it is possible to identify wave packets whose coherence length is much less than the separation between the measurement locations. The resulting dispersion is found to agree with theoretical results.

Keywords. Space Plasma Physics (Experimental and mathematical techniques; Wave-particle interactions; Waves and instabilities)

1 Introduction

The collisionless nature of space plasma means that plasma waves and turbulence play an integral role in the interactions between the various particle populations that exist within the plasma. They form the path by which energy may be exchanged between the ion species and also electrons. Thus, in order to understand these processes it is necessary to identify the various wave modes that exist within the plasma and also determine their characteristics. One key parameter to determine is the wave vector $\boldsymbol{k}$. The vector direction is the direction of propagation of the wave whilst its magnitude defines its wave number ($\boldsymbol{k}$) and is related to the wavelength (λ) by $k = 2\pi/\lambda$. Knowledge of the wave vector is often a crucial parameter that is required within theoretical descriptions of wave-particle interactions. For instance, theoretical studies of ElectroMagnetic Ion Cyclotron (EMIC) waves in the inner magnetosphere have shown that the EMIC waves may accelerate ions whose energy is proportional to the $\boldsymbol{k}$ vector (Pakhotin et al., 2013), lower hybrid waves may transfer energy between electrons and ions whose Larmor radii are of similar size to the components of the $\boldsymbol{k}$ vector in the direction parallel and perpendicular to the local magnetic field (e.g. Walker et al., 2008), whilst statistical properties of chorus emissions may be used to probe density irregularities along the wave path (Agapitov et al., 2010, 2011). Within the radiation belts, magnetosonic waves form an integral part of the mechanism to accelerate electrons to very high energies (Friedel et al., 2002; Horne et al., 2007). However, it is still unclear which external influence modulate the generation mechanism of these electrons (Reeves et al., 2011; Balikhin et al., 2011; Boynton et al., 2011).

The reconstruction of the wave vector depends upon the availability of simultaneous measurements at two or more closely spaced points in space. There are a number of possible methods that may be used to determine the wave vector, depending upon the available datasets, e.g. k filtering/wave telescope (Pinçon and Lefeuvre, 1992; Glassmeier et al., 2001), and phase differencing (Balikhin and Gedalin, 1993). However, all methods exploit the fact that at a particular frequency there will be a phase difference between the amplitudes at the points of measurement. Each of these methods has its advantages and disadvantages (Walker et al., 2004;

Pinçon and Glassmeier, 2008). For instance, the k filtering technique requires at least four point vector measurements and a longer time series whilst the phase differencing technique may be applied to scalar values and requires shorter intervals of data. However, the k filtering technique can successfully identify waves when more than one mode is present at a particular frequency. The two limitations of simultaneous observations and that the coherence length of the wave is larger than the separation of the measurement locations essentially restrict the applicability of such analyses to low frequency (MHD) waves. This paper discusses an extension to the phase differencing method to the identification of wave packets that are observed at separations much larger than the coherence length of the individual wave packets. Section 2 outlines the basic method used to determine the wave vector for cases when two point and multi-point (at least four) measurements are available. An extension to this method is described in Sect. 3 which enables the correlation of wave packets whose observations at different locations are temporally separated by a large number of wave periods. An example of the use of this method is shown in Sect. 4 based on the observation of packets of magnetosonic waves. Section 5 compares the experimentally determined wave vector to the theoretical dispersion curve and the results are summarised in Sect. 6.

2 Phase differencing

The phase differencing method assumes that in the plasma rest frame the wave field can be represented as the superposition of a number of plane waves.

$$\mathbf{B}(\boldsymbol{r},t) = \Sigma_\omega \mathbf{B}_\omega \exp[i(\boldsymbol{k}\cdot\boldsymbol{r} - \omega t)] + \text{cc} \tag{1}$$

where $\mathbf{B}_\omega$ is the wave amplitude at frequency ω, $\boldsymbol{k}$ is the wave vector ($\boldsymbol{k}$ vector), $\boldsymbol{r}$ is the separation vector between the location of the two (or more) simultaneous measurements, and cc represents the complex conjugate term. If the same wave is measured by two closely spaced satellites, then there will be a phase shift $\Delta\psi$ in one signal relative to the other. The magnitude of the phase shift is related to the component of the wave vector k_r projected along the separation direction $\boldsymbol{r}$ between the two measurement points by

$$\begin{aligned}\Delta\psi(\omega) &= \boldsymbol{k}(\omega)\cdot\boldsymbol{r} + 2n\pi \\ &= \|\boldsymbol{k}\|\|\boldsymbol{r}\|\cos(\theta_{kr}) + 2n\pi\end{aligned} \tag{2}$$

where θ_{kr} is the angle between the wave vector $\boldsymbol{k}$ and the satellite separation vector $\boldsymbol{r}$. The factor $2n\pi$ arises from the fact that the method will only determine the phase difference within the range $-2\pi < \Delta\psi < 2\pi$ and so result in a periodic family of solutions. Thus, it is important to ascertain the value of n in order to determine the actual projection of the $\boldsymbol{k}$ vector along the satellite separation vector (k_r) correctly. This is usually accomplished by inspection and comparison of the two waveforms. This point will be discussed more in the later sections of this paper.

The result of this analysis is a dispersion curve that shows a histogram of the measured amplitudes that occurred in the data period analysed as a function of the wave frequency and phase difference between the two measurements. From such a plot it is then straight forward to determine values of k_r as a function of frequency (Balikhin et al., 1997b; Chisham et al., 1999; Balikhin et al., 2001).

If data are measured at four (or more), non-coplanar points it is possible to reconstruct the complete $\boldsymbol{k}$ vector directly from its components k_r along three independent satellite separation directions (Balikhin et al., 2003). In this case,

$$\boldsymbol{k} = \mathbf{R}\cdot\boldsymbol{k}_r \tag{3}$$

where $\mathbf{R}$ is a matrix whose columns are the normalised separation vectors (Bates et al., 2000).

However, if such simultaneous datasets are unavailable it is still possible to reconstruct the full $\boldsymbol{k}$ vector if another method, such as variance analysis, may be used to determine its direction. This assumes that the wave is electromagnetic in nature, not linearly polarised, and that the analysis is applied to measurements of the magnetic field. In this case, the direction of propagation is defined by the minimum variance direction. It should be noted that there is an ambiguity of 180° in the direction of the minimum variance component. Its actual direction may be determined by comparing the two waveforms to see the order in which the spacecraft observed the wave and therefore deduce the constraint that this places in the propagation direction of the wave. Thus, the full $\boldsymbol{k}$ vector may be resolved using the direction determined from the variance analysis and its component measured along the satellite separation vector (Balikhin et al., 1997a).

3 Determination of n

As mentioned above, one of the key aspects to calculating the $\boldsymbol{k}$ vector using the phase differencing technique is to determine the value of n that appears in the phase ambiguity factor $2n\pi$ that appears in Eq. (2). In some cases, the value of n is obvious. Examples include the analysis of isolated wave packets that exist with no other wave activity occurring in the immediate vicinity. A good example of this was reported by Balikhin et al. (2005) who used this technique to identify the occurrence of ion sound waves in the foot of the quasiperpendicular shock front. In this case, the two waveforms could easily be matched and n determined. In such cases, n would be expected to take a small value, say $\|n\| < 5$. For low frequency waves, whose wavelength is larger than intersatellite separation distance, the value of n will be zero and also $\Delta\psi$ may be determined directly from the waveforms. In such cases, the branch of the dispersion curve passes through the origin ($k_r = 0, \omega = 0$) so that $n = 0$.

This then naturally invites the question regarding the possibility of determining n if the separation between measurement locations is large when compared to the wavelength of the waves. In such cases, the second satellite may observe the wave packet either at a separation distance corresponding to many wavelengths from the first satellite or after a time period that corresponds to many wave periods has elapsed assuming the satellite separation vector has a large angle to the $\boldsymbol{k}$ vector. So, how is it possible to determine the value of n in these cases? The key to answering this question is to examine the overall shape or envelope of the wave packet(s). Observations of the same wave packet at locations separated by a few 10's of wavelengths would be expected to exhibit similar structure provided the wave has not evolved a significant amount as it propagated through the intervening plasma. For an isolated wave packet it is straight forward to compare the two waveforms to establish that the measurement are of the same wave packet and then determine the time difference between similar features in the wave packet measured at different locations. Once the frequency of the wave packet is known, the value of n can be calculated easily. However, if a continuous series of wave packets are observed this becomes more problematic. Thus, in this paper an extension to the phase differencing technique, based upon the envelope of the waveform, is employed to determine the offset between the two datasets. There are a number of procedures that may be adopted to calculate the envelope of a waveform, typically taking the real waveform, reconstruct the complex part that is lost and then calculate the complex modulus or magnitude of the data. In this paper we use a method based upon wavelet transforms as opposed to the Hilbert transform. It should be noted, however, that both methods produced very similar results.

4 Example

The data used to illustrate this method were collected by the Cluster STAFF search coil magnetometer instruments (Cornilleau-Wehrlin et al., 1997) onboard spacecraft 1 and 2 on 13 March 2002 between 16:40 and 17:15 UTC. During this period, the Cluster satellites were situated in the inner magnetosphere at a geocentric distance of around 4.4 R_E on the night side (local time $\sim$ 00:50) and a magnetic latitude of $\approx 3°$ above the magnetic equator at the beginning of the period and moving in a northerly direction. Between 16:42 and 16:52 all Cluster satellites observed a general increase in wave activity in the frequency range 90–150 Hz. Examination of the STAFF propagation parameters (CAA data product not shown) reveal that these waves are typically propagating perpendicular to the external magnetic field and possess a high degree of ellipticity. These properties are typical of magnetosonic waves. It is also noticeable that the most intense emissions also exhibit a banded structure in the frequency range from $\approx$ 70 Hz up to $\approx$ 170 Hz, i.e. they are observed over a greater frequency range than the magnetosonic waves, similar to those reported by Russell et al. (1970) and Gurnett (1976). The background magnetic field was determined using data from the FGM instrument Balogh et al. (1997). Unfortunately, a data gap exists in the period of interest and so the background magnetic field vector was determined by smoothing the data using a one minute sliding window and then interpolating across the gap. This method appeared to produce more realistic result than those obtained from a model field. The actual difference in the total magnetic field resulting from the two methods was around 3 %. The field vector used in the subsequent analysis was (20, 137, 308) nT (magnitude 338 nT) in the GSE frame which results in a proton gyrofrequency around 5.2 Hz and an electron gyrofrequency of 9.5 kHz.

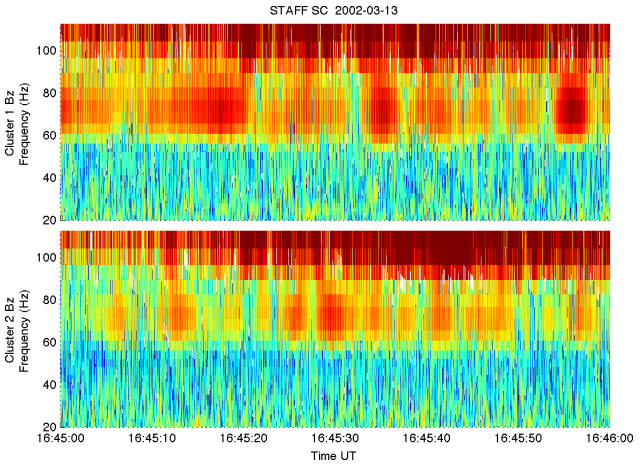

Fig. 1. Wavelet spectra of the magnetic field B_Z component measured by STAFF-SC onboard Cluster 1 (top) and Cluster 2 (bottom) showing a band of emissions centred around 70 Hz.

Figure 1 shows an example of the wave fluctuations detected by STAFF-SC (B_Z component) on satellites 1 (top) and 2 (bottom) between 16:45 and 16:46 UTC on 13 March 2002. As mentioned above, the main magnetosonic emissions occur from around 90 Hz and above and are seen in the top of each panel. Below this frequency, there is a band of intermittent wave activity occurring centred around 70 Hz. Each of these periods of emissions consists of a series of individual wave packets. It is evident that due to the fairly continuous nature of the emissions, it is impossible to correlate the occurrence of individual wave packets. To do this successfully, the data should be examined on a much finer time scale and compare the packet structure or amplitude envelope in order to determine the time difference between the observations and hence the n, the number of wave periods. To examine the structure of these wave packets in more detail the data were first filtered at a frequency around 70 Hz using the complex Morlet wavelet (Eq. 4) with gaussian width 1 (Dudok de Wit et al., 1995).

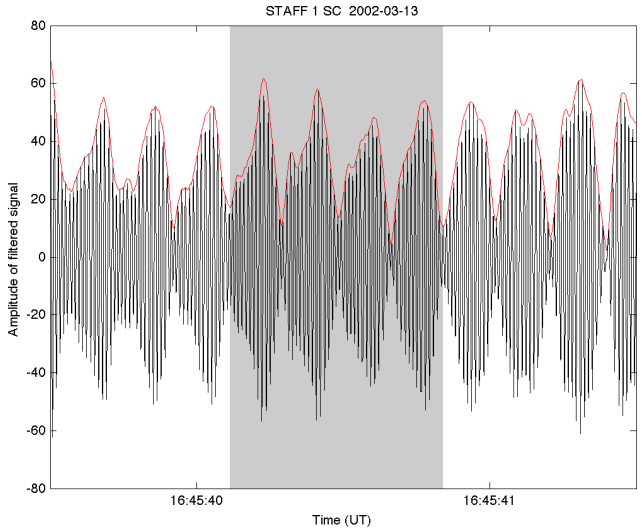

Fig. 2. Structure of wave packets observed by Cluster 1 on 13 March 2002 between 16:45:39.5 and 16:45:41.5 UTC.

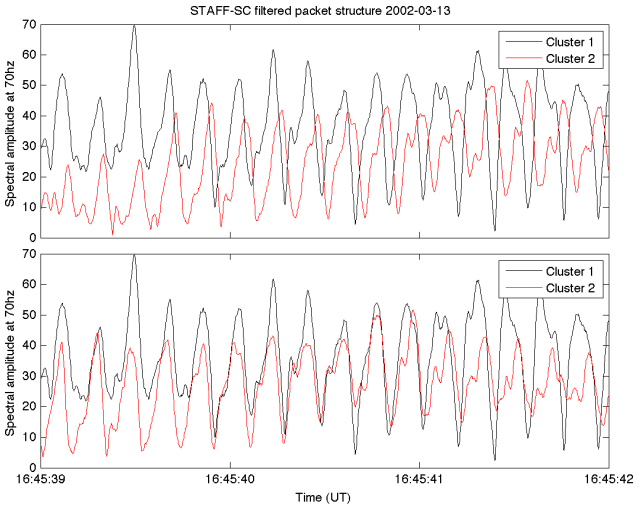

Fig. 3. Structure of wave packets observed by Cluster 1 (black) and Cluster 2 (red) on 13 March 2002 between 16:45:39.5 and 16:45:41.5 UTC. In the top panel the two series are shown with their original time tags. In the lower panel, the Cluster 2 data has been shifted by 604 ms to align it with the Cluster 1 measurements.

$$h(t) = \frac{1}{\pi^{1/4}} \exp(-2\pi i t) \exp(-t^2/2) \quad (4)$$

The resulting filtered waveform is complex in nature. The amplitude profile, or envelope, of these packets may then be calculated using the complex modulus of the filtered data. An example of the waveform and its packet structure is shown in Fig. 2. The black line is the 70 Hz filtered B_Z waveform measured by STAFF-SC on spacecraft 1. It clearly shows the packet nature of the emissions. The red line shows the outline packet structure (modulus of the complex data). This clearly shows the fact that every packet has a slightly different shaped envelope depending upon the phases of the beat frequencies. Thus, in order to determine the phase offset n between the two measurement locations a comparison is required based on the packet structures of the two measurements. The grey region of Fig. 2 highlights four consecutive wave packets whose envelope shapes are quite distinctive. These packets form the basis for the comparison between the two datasets.

Figure 3 shows the shape of the packet envelopes for Cluster 1 (black) and Cluster 2 (red). In the top panel both quantities are plotted against their own time tags. There is no clear correlation between the structures of the wave packets shown in this panel. They are completely different. However, on closer inspection it is clearly seen that some of the wave packets observed by Cluster 1 bear a striking resemblance to packets observed by Cluster 2 around 0.6 s later. A cross correlation analysis was performed using the envelope data to determine an approximate time offset. The exact time offset was then calculated based on the waveforms of the packets under study. The lower panel of Fig. 3 compares the packet structures after a timing offset of −604 ms has been applied to Cluster 2 (the time axis refers to Cluster 1). In this case there is a very good correlation between the two datasets with many of the features observed by Cluster 1 also observed in the Cluster 2 data. Thus, it appears as if Cluster 2 sees the same wave packets as Cluster 1 with a time delay of around 600 ms. This corresponds to around 42 periods of a wave with frequency 70 Hz.

To determine the exact delay the waveforms of the packets in question should be compared. By adjusting the timing offset applied to the Cluster 2 data it was found that the exact time difference between the two datasets was −604 ms, which corresponds to −42.28 wave periods. Figure 4 compares the waveforms of the packets highlighted in Fig. 2 as observed by Cluster 1 (black) and Cluster 2 (red) 604 ms later. It is clear that these are indeed the same wave packets measured by the two satellites.

Using a time offset of −600 ms (which corresponds to 42 periods of a 70 Hz wave) for the Cluster 2 data the $\omega - k$ dispersion was computed using the phase differencing technique. From the analysis presented above it was determined that the exact time offset was 604 ms which corresponds to 42.28 wave periods. Therefore, the results of the phase differencing calculations should show a peak at around −1.75 rads at a frequency of 70 Hz. The results of the analysis, shown in Fig. 5, do indeed show a peak at this location in $\omega - k$ space. Further examination of Fig. 4 shows that whilst the maximal amplitudes of the wave packets coincide, the minima between the packets may show a phase variation of up to $\pi/2$. This effect will make the dispersion branches shown in Fig. 5 to widen and hence result is slightly larger errors. However, the main result would be unaffected.

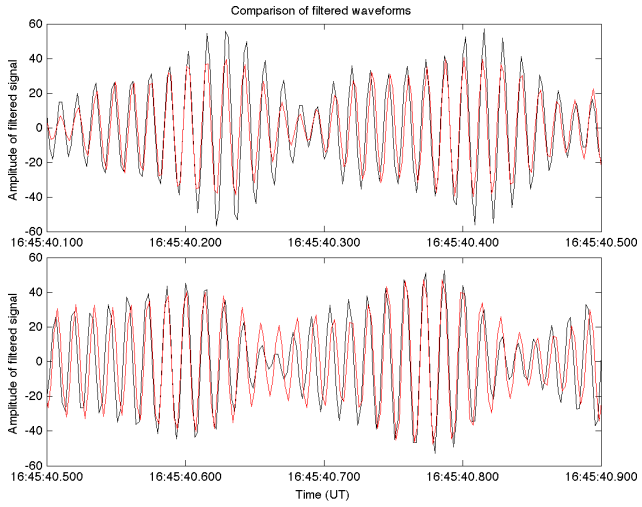

Fig. 4. A comparison of two wave packets measured by Cluster 1 and Cluster 2 with a time offset of 604 ms.

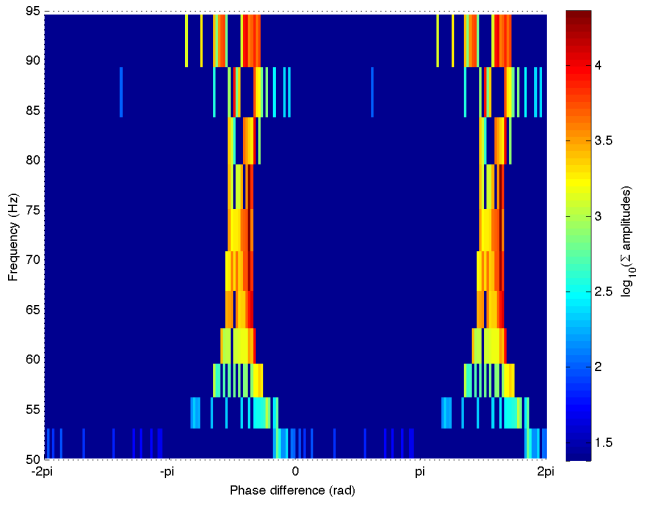

Fig. 5. The $\omega - k$ dispersion function calculated using Cluster 2 data with a time offset of 600 ms.

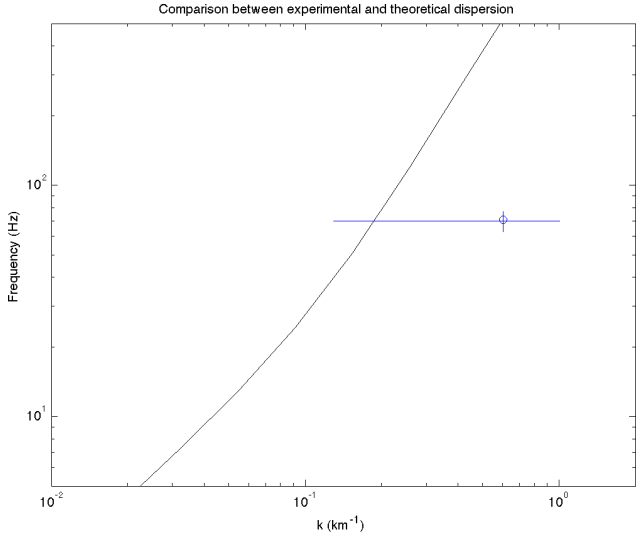

Fig. 6. Comparison of experimental and theoretical results.

For this example, the direction of the $\boldsymbol{k}$ vector was determined from the STAFF spectral matrix data available from CAA. In science burst mode, this dataset provides the full spectral matrix for 18 frequencies in the range 70 Hz–4 kHz at a time resolution of 1 s. Thus, the resulting direction will be the average of all wave activity during this period. The wave vector direction was calculated based on the values of the spectral matrix using the methods of McPherron et al. (1972) and Santolik et al. (2003) to be (0.12, −0.99, 0.002). This direction lies almost perpendicular to the background magnetic field ($\theta_{Bk} = 83°$). However, it should be noted that the ratio of the intermediate to lowest eigenvalue determined during this calculation was in the range 2–3, which implies that the minimum variance direction is not resolved particularly accurately. The error in direction, estimated using the method of Hoppe et al. (1981) is $> 20°$. This represents the major source of error in the following calculations. Never the less, these values will be used for the example calculation.

Since the measured value of k_r represents the projection of the $\boldsymbol{k}$ vector onto the satellite separation direction the full $\boldsymbol{k}$ vector may be reconstructed using Eq. (3). From the calculations above, the observed phase difference is $42.28 \times 2 \times \pi$ rad. The separation vector between satellites 1 and 2 was (12.8, −40.0, −182.6) km (GSE) and thus $\theta_{kr} = 64°$. Thus, the magnitude of the wave vector $k \sim 0.3\,\mathrm{km}^{-1}$.

5 Comparison with theory

Magnetosonic waves are electromagnetic emissions that are often observed within 3° of the magnetic equator, between $2 \leq L \leq 7$, and 10–22 MLT. They occur in the frequency band between the proton gyrofrequency and the lower hybrid resonance frequency and are thought to be generated by instabilities associated with a ring distribution of energetic protons of the order of 10 keV (Horne et al., 2007; Chen and Thorne, 2012). The waves themselves propagate at angles approximately perpendicular to the magnetic field ($\theta_{Bk} \sim 89°$) and are elliptically polarised with an ellipticity of ≈ 0. The dispersion relation, derived using the cold plasma approximation and assuming that $\omega_{\mathrm{pe}}^2 \gg \Omega_{\mathrm{e}}^2$ and $\Omega_{\mathrm{i}}^2 \ll \omega \ll \Omega_{\mathrm{e}}^2$, where ω_{pe}^2 is the electron plasma frequency and $\Omega_{\mathrm{e(i)}}^2$ is the electron (ion) cyclotron frequency, may be written as (Musher and Sturman, 1975)

$$\frac{\omega^2}{\Omega_{\mathrm{e}}^2} = \left(\frac{k_\parallel^2}{1 + k_\perp^2} + \frac{\omega_{\mathrm{LH}}^2}{\Omega_{\mathrm{e}}^2} \right) \frac{k^2}{1 + k^2} \tag{5}$$

where $\omega_{\mathrm{LH}}^2 = \Omega_{\mathrm{e}} \Omega_{\mathrm{i}}$ is the lower hybrid resonance frequency and $k^2 = k_\parallel^2 + k_\perp^2$ is the wave vector normalised to the

electron inertial length. Figure 6 shows a section of the magnetosonic dispersion curve calculated using Eq. (5). The magnitude of the $\boldsymbol{k}$ vector determined above, represented by the circle, lies close to this curve, indicating that the wave type analysed is most probably a magnetosonic mode. As noted above, the major source of errors in the determination of $\boldsymbol{k}$ is related to the inaccuracies in the determination of the minimum variance direction.

6 Summary

This paper has discussed a method to establish the phase difference between wave packets that are observed by two spacecraft at times separated by a large number of wave periods. The key is to match the two wave packets in question by first analysing the shape of the wave packet envelopes to determine the approximate time difference between the two observations of the same wave packet. This step of the analysis extends the usage of the phase differencing technique to wave packets that are observed at similar times, i.e. observed within a few wave periods in contrast to previous studies that were restricted to simultaneous observations. This method was then applied to the identification of wave packets observed in the vicinity of the magnetic equator. It was shown that there wave are probably magnetosonic in nature since the experimentally determined value of the $\|k\|$ lies extremely close to the magnetosonic branch of the dispersion relation.

Acknowledgements. The authors wish to thank the Cluster STAFF and FGM teams for making their data available through the Cluster Active Archive. This joint study was funded in the framework of a Royal Society International Collaboration grant. SNW is grateful to STFC for financial support.

Topical Editor M. Gedalin thanks two anonymous referees for their help in evaluating this paper.

References

Agapitov, O., Krasnoselskikh, V., Zaliznyak, Yu., Angelopoulos, V., Le Contel, O., and Rolland, G.: Chorus source region localization in the Earth's outer magnetosphere using THEMIS measurements, Ann. Geophys., 28, 1377–1386, doi:10.5194/angeo-28-1377-2010, 2010.

Agapitov, O., Krasnoselskikh, V., Dudok de Wit, T., Khotyaintsev, Y., Pickett, J. S., Santolík, O., and Rolland, G.: Multispacecraft observations of chorus emissions as a tool for the plasma density fluctuations remote sensing, J. Geophys. Res., 116, A09222, doi:10.1029/2011JA016540, 2011.

Balikhin, M. A. and Gedalin, M. E.: Comparative analysis of different methods for distinguishing temporal and spatial variations, in: Proc. of START Conf., Aussois, France, Vol. ESA WPP 047, 183–187, 1993.

Balikhin, M. A., Dudok de Witt, T., Woolliscroft, L. J. C., Walker, S. N., Alleyne, H., Krasnoselskikh, V., Mier-Jedrzejowicz, W. A. C., and Baumjohann, W.: Experimental determination of the dispersion of waves observed upstream of a quasi–perpendicular shock, Geophys. Res. Lett., 24, 787–790, doi:10.1029/97GL00671, 1997a.

Balikhin, M. A., Walker, S. N., Dudok de Witt, T., Alleyne, H. S., Woolliscroft, L. J. C., Mier-Jedrzejowicz, W. A. C., and Baumjohann, W.: Nonstationarity and Low Frequency Turbulence at a Quasi-perpendicular Shock Front, Adv. Sp. Res., 20, 729–734, doi:10.1016/S0273-1177(97)00463-8, 1997b.

Balikhin, M. A., Schwartz, S., Walker, S. N., Alleyne, H. S. C. K., Dunlop, M., and Lühr, H.: Dual-spacecraft observations of standing waves in the magnetosheath, J. Geophys. Res., 106, 25395–25408, doi:10.1029/2000JA900096, 2001.

Balikhin, M. A., Pokhotelov, O. A., Walker, S. N., Amata, E., Andre, M., Dunlop, M., and Alleyne, H. S. K.: Minimum variance free wave identification: Application to Cluster electric field data in the magnetosheath, Geophys. Res. Lett., 30, 1508, doi:10.1029/2003GL016918, 2003.

Balikhin, M., Walker, S., Treumann, R., Alleyne, H., Krasnoselskikh, V., Gedalin, M., Andre, M., Dunlop, M., and Fazakerley, A.: Ion sound wave packets at the quasiperpendicular shock front, Geophys. Res. Lett., 32, L24106, doi:10.1029/2005GL024660, 2005.

Balikhin, M. A., Boynton, R. J., Walker, S. N., Borovsky, J. E., Billings, S. A., and Wei, H. L.: Using the NARMAX approach to model the evolution of energetic electrons fluxes at geostationary orbit, Geophys. Res. Lett., 38, L18105, doi:10.1029/2011GL048980, 2011.

Balogh, A., Dunlop, M. W., Cowley, S. W. H., Southwood, D. J., Thomlinson, J. G., Glassmeier, K. H., Musmann, G., Lühr, H., Buchert, S., Acuña, M. H., Fairfield, D. H., Slavin, J. A., Riedler, W., Schwingenschuh, K., and Kivelson, M. G.: The Cluster Magnetic Field Investigation, Space Sci. Rev., 79, 65–91, doi:10.1023/A:1004970907748, 1997.

Bates, I., Balikhin, M., Alleyne, H. S., Dunlop, M., and Lühr, H.: Coherence Lengths of the Low Frequency Turbulence at the Bow Shock and in the Magnetosheath, in: Proceedings of the Cluster-II Workshop Multiscale/Multipoint Plasma Measurements, 22–24 September 1999, Imperial College, London, UK, edited by: Balough, A., Escoubet, C. P., and Harris, R. A., Vol. ESA SP-449, p. 283, 2000.

Boynton, R. J., Balikhin, M. A., Billings, S. A., Wei, H. L., and Ganushkina, N.: Using the NARMAX OLS-ERR algorithm to obtain the most influential coupling functions that affect the evolution of the magnetosphere, J. Geophys. Res. Space Phys., 116, A05218, doi:10.1029/2010JA015505, 2011.

Chen, L. and Thorne, R. M.: Perpendicular propagation of magnetosonic waves, Geophys. Res. Lett., 39, L14102, doi:10.1029/2012GL052485, 2012.

Chisham, G., Schwartz, S. J., Balikhin, M., and Dunlop, M. W.: AMPTE observations of mirror mode waves in the Magnetosheath: Wavevector determination, J. Geophys. Res. A, 104, 437–447, doi:10.1029/1998JA900044, 1999.

Cornilleau-Wehrlin, N., Chauveau, P., Louis, S., Meyer, A., Nappa, J. M., Perraut, S., Rezeau, L., Robert, P., Roux, A., De Villedary, C., de Conchy, Y., Friel, L., Harvey, C. C., Hubert, D., Lacombe, C., Manning, R., Wouters, F., Lefeuvre, F., Parrot, M., Pinçon, J. L., Poirier, B., Kofman, W., Louarn, P., and the STAFF Investigator Team: The Cluster Spatio-Temporal Analysis of Field

Fluctuations (Staff) Experiment, Space Sci. Rev., 79, 107–136, 1997.

Dudok de Wit, T., Krasnoselskikh, V. V., Bale, S. D., Dunlop, M. W., Lühr, H., Schwartz, S. J., and Woolliscroft, L. J. C.: Determination of dispersion relations in quasi–stationary plasma turbulence using dual satellite data, Geophys. Res. Lett., 22, 2653–2656, doi:10.1029/95GL02543, 1995.

Friedel, R. H. W., Reeves, G. D., and Obara, T.: Relativistic electron dynamics in the inner magnetosphere – a review, J. Atmos. Sol. Terr. Phys., 64, 265–282, doi:10.1016/S1364-6826(01)00088-8, 2002.

Glassmeier, K.-H., Motschmann, U., Dunlop, M., Balogh, A., Acuña, M. H., Carr, C., Musmann, G., Fornaçon, K.-H., Schweda, K., Vogt, J., Georgescu, E., and Buchert, S.: Cluster as a wave telescope – first results from the fluxgate magnetometer, Ann. Geophys., 19, 1439–1447, doi:10.5194/angeo-19-1439-2001, 2001.

Gurnett, D. A.: Plasma wave interactions with energetic ions near the magnetic equator, J. Geophys. Res., 81, 2765–2770, doi:10.1029/JA081i016p02765, 1976.

Hoppe, M. M., Russell, C. T., Frank, L. A., Eastman, T. E., and Greenstadt, E. W.: Upstream hydrodynamic waves and their association with back streaming ion populations: ISEE 1 and 2 observations, J. Geophys. Res. A, 86, 4471–4492, 1981.

Horne, R. B., Thorne, R. M., Glauert, S. A., Meredith, N. P., Pokhotelov, D., and Santolík, O.: Electron acceleration in the Van Allen radiation belts by fast magnetosonic waves, Geophys. Res. Lett., 34, L17107, doi:10.1029/2007GL030267, 2007.

McPherron, R. L., Russell, C. T., and Coleman Jr., P. J.: Fluctuating Magnetic Fields in the Magnetosphere. II: ULF Waves, Space Sci. Rev., 13, 411–454, doi:10.1007/BF00219165, 1972.

Musher, S. L. and Sturman, B. I.: Collapse of plasma waves near the lower hybrid resonance, Sov. Phys.-JETP, 22, 537–542, 1975.

Pakhotin, I. P., Walker, S. N., Shprits, Y. Y., and Balikhin, M. A.: Dispersion relation of EMIC waves using Cluster data, Ann. Geophys., in press, 2013.

Pinçon, J.-L. and Glassmeier, K.-H.: Multi-Spacecraft Methods of Wave Field Characterisation, ISSI Scientific Reports Series, 8, 47–54, 2008.

Pinçon, J.-L. and Lefeuvre, F.: The application of the generalized Capon method to the analysis of a turbulent field in space plasma: Experimental constraints, J. Atmos. Terr. Phys., 54, 1237–1247, 1992.

Reeves, G. D., Morley, S. K., Friedel, R. H. W., Henderson, M. G., Cayton, T. E., Cunningham, G., Blake, J. B., Christensen, R. A., and Thomsen, D.: On the relationship between relativistic electron flux and solar wind velocity: Paulikas and Blake revisited, J. Geophys. Res. Space Phys., 116, A02213, doi:10.1029/2010JA015735, 2011.

Russell, C. T., Holzer, R. E., and Smith, E. J.: OGO 3 observations of ELF noise in the magnetosphere: 2. The nature of the equatorial noise, J. Geophys. Res., 75, 755–768, doi:10.1029/JA075i004p00755, 1970.

Santolik, O., Parrot, M., and Lefeuvre, F.: Singular value decomposition methods for wave propagation analysis, Radio Sci., 38, 10–1, doi:10.1029/2000RS002523, 2003.

Walker, S. N., Sahraoui, F., Balikhin, M. A., Belmont, G., Pinçon, J. L., Rezeau, L., Alleyne, H., Cornilleau-Wehrlin, N., and André, M.: A comparison of wave mode identification techniques, Ann. Geophys., 22, 3021–3032, doi:10.5194/angeo-22-3021-2004, 2004.

Walker, S. N., Balikhin, M. A., Alleyne, H. St. C. K., Hobara, Y., André, M., and Dunlop, M. W.: Lower hybrid waves at the shock front: a reassessment, Ann. Geophys., 26, 699–707, doi:10.5194/angeo-26-699-2008, 2008.